Microelectronic Engineering 124 (2014) 66–75

Contents lists available at ScienceDirect

Microelectronic Engineering

journal homepage: www.elsevier.com/locate/mee

The improved resistance of PDMS to pressure-induced deformation and chemical solvent swelling for microfluidic devices

Myeongsub "Mike" Kim [a], Yu Huang [a], Kevin Choi [a], Carlos H. Hidrovo [b,*]

[a] Mechanical Engineering Department, University of Texas at Austin, Austin, TX 78712, USA
[b] Mechanical and Industrial Engineering Department, Northeastern University, Boston, MA 02115, USA

ARTICLE INFO

Article history:
Received 28 October 2013
Received in revised form 22 February 2014
Accepted 9 April 2014
Available online 6 May 2014

Keywords:
PDMS
Deformation
Pressure-driven flow
Chemical swelling
Dye diffusion
Microfluidic devices

ABSTRACT

We present a fabrication technique that increases the resistance of PDMS to deformation under pressure driven flow and chemical solvents swelling without the use of any foreign materials. This is achieved by enhancing the material properties of PDMS by coupling two previously isolated processes. First, the weight ratio of the prepolymer to the curing agent was increased from 10:1 to 5:1, with the latter showing 20% less deformation under pressurized conditions. Second, the cured PDMS was thermally aged at 200 °C for a few hours, resulting in 140% less deformation for the thermally aged chip under the same pressure conditions. The combined processes benefit from a nonlinear coupling effect on improvement and show 860% less deformation under pressure driven flow in the enhanced PDMS chip compared to that in the standard 10:1 PDMS chip. The deformation of the standard and the enhanced PDMS microchannels under pressure driven flow is quantified using fluorescence microscopy. The compatibility of PDMS with nonpolar solvents was also explored by quantifying material swelling due to toluene absorption using brightfield imaging of the microchannel. The enhanced PDMS showed less than 10% swelling against toluene compared to 55% in the standard PDMS. The enhanced PDMS is also less permeable to the small hydrophobic molecule rhodamine B (RhB), as quantified by epi-fluorescence microscopy of the absorbed dye. The improved surface and material properties of the thermally treated PDMS are certainly beneficial in microfluidic applications that use this common soft lithography material.

1. Introduction

The exponential growth of soft lithography microfabrication techniques for Lab-on-a-Chip and micro-Total Analysis System applications makes polydimethylsiloxane (PDMS) the most common material for microfluidic devices due to its easy, rapid, and low cost fabrication, biocompatibility, and transparent properties [1–5]. The range of applications for PDMS-based devices requires broad geometrical shapes from simple straight channels to complicated geometries including high or low aspect ratio channels [6–8]. In addition, PDMS allows fabrication of feature sizes from the macroscale to the microscale, and even to the nanometer scale, providing further flexibility in geometry control [9–11].

Despite these advantages, the intrinsic properties of PDMS hinder this material in various microfluidic applications [12]. First, the typical Young's modulus of 10:1 PDMS remains less than 1.35 MPa [13], making PDMS structures highly compliant and flexible [14,15]. The high compliancy becomes especially problematic in channels with extreme aspect ratios under pressure-driven flow [16–18]. Gervais et al. [19] experimentally investigated the deformation of low aspect ratio (20:1 = width:height) PDMS microchannels at flow rates as high as 1500 μL/min and measured velocity profiles in the laminar region, with pressure distribution through the microchannels inferred from its deformation, which was assessed using confocal microscopy. They showed that shallower channels were significantly deformed at high pressures (up to 1.5 bar), and exhibited larger deviations than expected from given pressure drops and flow rates compared to rigid square channels. A few other studies have also shown that the deformed PDMS microchannels under pressure driven flows lead to significant errors in theoretical and computational analysis of the flows in the microfluidic systems [20–23].

To characterize PDMS deformation, focus has been placed on theoretical analysis, including the flexible tube model [24] as well as the finite element method in elastic tubes [25]. In addition, several experimental studies of the deformation have also been conducted. The changes in cross-sectional area due to bulging of PDMS microchannels at flow rates of 15–1500 nL/min were experimentally measured by fluorescence microscopy and used to

* Corresponding author. Tel.: +1 617 373 7520.
E-mail address: hidrovo@neu.edu (C.H. Hidrovo).

http://dx.doi.org/10.1016/j.mee.2014.04.041
0167-9317/

determine theoretical concentration gradients in a microfluidic diffusion diluter [26]. Gervais et al. [19] used confocal microscopy to study the elastic deformation of PDMS channels at various flow rates and found that, for a given pressure drop, the measured flow rates in the deformed channels were 500% higher compared to that in rigid channels. Hardy et al. [21] further engineered the method of fluorescence microscopy to quantify the deformation of shallow channels (13.5:1 = width:height) along the optical axis of the imaging system. They specifically investigated the relationship between wall thickness and channel deformation under pressure driven flow and obtained a 35% decrease in pressure drop in the deformed channel compared to that in the rigid-walled channel. While the previous theoretical and experimental investigations provide insight into the effects of channel deformation on the flow rates and pressure drops in PDMS channels, their studies are limited to just verifying the measurement errors of pressure drops and flowrates due to the channel deformation. Therefore, methods that directly enhance the material properties of PDMS channels to reduce their deformation under pressure-driven flow conditions and improve the accuracy of the flow measurements are quite useful.

Another aspect of using PDMS in the fabrication of microfluidic devices is that some organic solvents such as hexadecance, dichloromethane, and toluene swell PDMS substantially, degrading device performance and making the use of PDMS limited in solvent manipulation applications [27–31]. Lee et al. [32] experimentally measured the degree of swelling of PDMS with several solvents including diisopropylamine, trithylamine, pentane, and xylenes. They grouped the solvents into four classifications in terms of the solubility effect on PDMS and observed a maximum of 20% change in channel width due to swelling. Dangla et al. [33] quantitatively measured the PDMS microchannel deformation through changes in the channel height using a synthetic Schlieren approach when PDMS was in contact with swelling solvents. They showed that hexadecane swelled PDMS as much as 14% when compared to a dry channel. Although swelling is desirable in a few applications such as extraction of uncross-linked oligomers [32], channel deformation due to swelling often results in inaccurate measurements of flow rates and pressure drops.

The enhancement of inherent material properties of PDMS can mitigate these disadvantages, i.e., large deformation under pressure-driven flow and significant swelling due to chemical contacts. First of all, to reduce the pressure-induced deformation, the stiffness of a PDMS channel should be increased while maintaining its optical properties. The enhanced stiffness of PDMS can be achieved by an increased amount of the curing agent during mixing [34]. Park et al. [34] obtained a 40% increase in PDMS stiffness when the mixing ratio was doubled. The increase of PDMS stiffness is also possible by thermally aging it at high temperature for a long period of time. Fuard et al. [15] cured and aged 10:1 PDMS at 100 °C for 7 days, resulting in a 40% increase in PDMS stiffness. By combining and modifying these two methods, we have further improved PDMS properties. On the other hand, to enhance the surface properties of PDMS, and further increase its chemical resistance, there are a few methods available [29,30,35–39]. For example, Abate et al. [28] developed a sol–gel technique that improves chemical resistance of PDMS channels and controls surface properties by coating the PDMS with a glass layer. Thin layers of fluoropolymer coatings through initiated chemical vapor deposition [36] and combination of a solution-phase oxidation and subsequent silanization reactions [37] were other possible means to increase the chemical compatibility of PDMS. However, all these methods require the introduction of foreign materials and multistep chemical synthesis as post fabrication.

In this paper, we demonstrate a fabrication method of PDMS channels that improves material properties without involving foreign materials or complicated post processing. This method enhances the material properties of PDMS offering significantly less deformation under pressure driven flows compared to conventional PDMS channels, and the enhanced PDMS also considerably increases its chemical resistance to organic solvents providing strong impediment to swelling. The enhanced properties of PDMS were achieved by combining and modifying previously isolated approaches into an integrated process: (1) increased mixing ratio during PDMS curing and (2) thermal treatment of cured PDMS. This method does not use any chemicals and can be completed within a few hours. Using the compounded approach of increased mixing ratio of 5:1 coupled with a subsequent thermal treatment, the resistance to pressure-induced deformation of PDMS was improved up to 860%, which is an exceptional nonlinear increment. This is the highest improvement in PDMS resistance to deformation without using surface treatments or alien materials. The enhanced properties of thermally aged 5:1 PDMS also provide a good hindrance to dye absorption, which was 41.6% less permeable than the conventional 10:1 PDMS channels.

2. Materials and methods

2.1. PDMS chip fabrication

Si wafers containing microchannel geometries were prepared by standard photolithography [2]. Briefly, a plain polished 4-inch Si wafer was thoroughly cleaned by acetone and isopropanol (IPA) subsequently. A negative photoresist SU-8 2025 (Microchem, MA, USA) was spun at 2000–3000 rpm for 45 s with a thickness of 30–100 μm accordingly. The coated Si wafer was baked at 65 °C for 4–8 min and subsequently at 85 °C for 6–10 min according to the SU8 thickness. Following the UV exposure of the Si wafer for 18 s, the wafer was baked again at 65 °C for 3–5 min and at 85 °C for 4–8 min. The baked silicon wafer was then developed for 3–10 min.

PDMS channels at the two different mixing ratios, 10:1 (w/w) and 5:1 (w/w), were molded in two different methods. For 10:1 PDMS chips, the sylgard 184 prepolymer (Dow corning, USA) and the curing agent were well mixed in a plastic cup at a weight ratio of 10:1. The mixture was poured on the patterned silicon wafer and degassed for 40 min to remove air bubbles formed during mixing. The mixture was then cured at 85 °C for 35 min. Once cured, the PDMS mold was carefully peeled off from the Si wafer. The inlet and outlet holes were then punched for the tubing connection. Both the PDMS mold and glass substrate were treated by plasma for 90 s and brought together into conformal contact for bonding. For 5:1 PDMS, the mixing ratio of 5:1 was used and the mixture was cured at 85 °C for 35 min. After curing, the mold was peeled off from the Si wafer and the puncher made holes for inlet and outlet reservoirs. The same procedure was taken for plasma bonding. Then, the bonded chip was placed onto the glass substrate for thermal treatment on the hot plate.

Low and high temperatures of 85 °C and 250 °C, respectively, were initially chosen for thermal treatment comparison. It was found that thermal treatment at temperatures higher than 200 °C provides very little additional increase in Young's modulus and hardness of PDMS at a given mixing ratio, with less than 1% deviation in these properties above this temperature.

2.2. Channel deformation measurements

Fluorescence microscopy is employed to quantify the channel deformation by correlating the fluorescein's emission intensities to the channel deformation. The working fluid was an aqueous 10 μM fluorescein (FL) solution in deionized (DI) water, delivered

by a syringe pump (Harvard Instrument, USA) at various volume flow rates ranging from 0 to 200 μL/min. A concentration 10 μM was chosen to stay in the optically thin regime so that intensity and deformation are linearly related [21]. While a syringe containing the 20 mL of working fluid injected the solution, fluorescence images were taken through an upright optical microscope (LV100, Nikon). A 50 mW argon ion laser illuminated the FL solution at 488 nm. A bandpass filter (500–550 nm) and 10× microscope objective was used to collect the FL emission in the CCD camera.

2.3. Swelling of PDMS channels

Toluene, an organic solvent that significantly swells PDMS [28,30,32], was delivered to 10:1, 5:1, and thermally treated 5:1 PDMS chips at 20 μL/min using a glass syringe pump. A built-in 50 W halogen lamp was used as a light source. Before the toluene injection, an image of the original channel at $t = 0$ was taken to serve as the initial reference size. Once the channel was filled with toluene, the images were taken at 40 ms exposure at 7 frames per second to estimate the evolution of channel geometry due to swelling.

2.4. Diffusion of rhodamine B into PDMS

PDMS is a material permeable to gas and organic molecules [40–42]. Rhodamine B (RhB), an organic fluorescent dye that diffuses into cured PDMS, was used as an indicator for measurements of diffusion and absorption of RhB to PDMS. After curing both 10:1 and 5:1 PDMS channels, they were placed on the microscope stage such that the field of view was the same for each chip. The 100 μM aqueous RhB solution was then injected by the syringe pump at 10 μL/min. A reference image at $t = 0$ s was taken immediately after the solution was injected and the sequence of images were taken at every 10 min to monitor the dye absorption and diffusion into PDMS. Fluorescence emissions from RhB solution were filtered out using a 520–580 nm bandpass filter and recorded onto the CCD camera using a 10× objective lens.

3. Results and discussion

3.1. Channel deformation under pressure driven flows

The deformation of PDMS channel under pressure driven flow was investigated in six different channels, as shown in Table 1. For simplicity, the channels are named according to their mixing ratios and heat treatment as following: 10:1 PDMS with no thermal treatment (M10T0), 5:1 PDMS with no thermal treatment (M5T0), thermally treated 10:1 PDMS at 200 °C for 1 day (M10T1), thermally treated 5:1 PDMS at 200 °C for 1 day (M5T1), thermally treated 10:1 PDMS at 200 °C for 3 days (M10T3), and thermally treated 5:1 PDMS at 200 °C for 3 days (M5T3). These channels are straight and have a cross-section of 400 μm (width) × 40 μm (height) with a length of 50 mm, as shown in Fig. 1a.

Table 1
Symbolized terms of the different PDMS channels used in this study. M and T represent the mixing ratio and thermal treatment, respectively.

Heat treatment	Mixing ratio (prepolymer: curing agent)	
	10:1	5:1
No thermal treatment	M10T0	M5T0
200 °C for 1 day	M10T1	M5T1
200 °C for 3 days	M10T3	M5T3

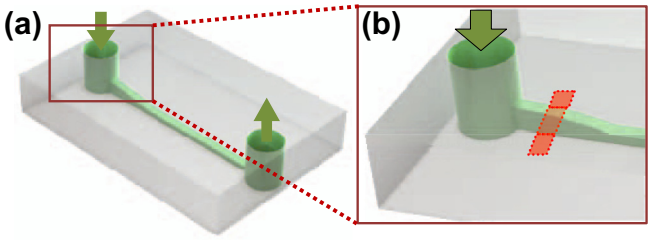

Fig. 1. (a) PDMS channel geometry for deformation tests under pressure driven flow. (b) Exploded view of the channel close to the inlet reservoir. Red dotted region represents the location where the fluorescence imaging was performed. Arrows represent the flow direction. (For interpretation of the references to color in this figure legend, the reader is referred to the web version of this article.)

To check the fully developed condition of the flow, entrance lengths (l_e) for these flow rates were calculated based on the well-known formula [43]:

$$l_e = 0.06 \mathrm{Re} D \tag{1}$$

where D is the hydraulic diameter of the non-circular cross-section channel. Note that the flows at all flow rates tested are in the laminar regime (Re < 1.6). The calculated entrance lengths are less than 7 μm. Comparing 7 μm of the entrance length with 50 mm of the entire channel length, we assume the flow in the entire channel is fully developed and use the Eq. (2) to calculate pressure drop [43].

$$\Delta P = \frac{\pi D^4 Q}{128 \mu L} \tag{2}$$

where D is the hydraulic diameter, Q is the volume flow rate, μ is the dynamic viscosity of the fluid, and L is the length of the channel. The outlet of the channel was opened to atmospheric condition. From the theoretical linear pressure drop for laminar flow in a straight rigid channel, the location of the highest pressure in the channel is assumed to be near the inlet reservoir. Therefore, the pressures at the channel inlet are 117, 133, and 165 kPa at the flow rates of 50, 100, and 200 μL/min, respectively.

The fluorescence images were taken at fully developed region 2.5 mm away from the inlet reservoir (red rectangular section in Fig. 1b) using FL as a tracer. The concentration used here satisfies the optically thin condition, so at a constant solution concentration the fluorescence intensity measured possesses the linear relationship with fluorescence dye layer thickness (i.e., channel depth) [44]. Hence, the linear relationship between FL emission and the depth of FL solution allows measurements of the channel deformation induced by the pressure drop. Fig. 2 shows raw fluorescence images of the channels at the flow rate of $Q = 0$ (Fig. 2a) and $Q = 200$ μL/min (Fig. 2b). The rectangle delineated by a red dotted line represents the region where FL intensities were averaged in order to estimate the deformation. After spatially averaged over the rectangle region along x direction, the intensity profiles between the no flow and flow conditions were compared to each other to estimate changes in channel depth (i.e., intensity) and width. We found that the variations in channel width due to the pressure-driven flow were negligible. Compared to the no flow condition, high intensities were observed at the centre region at $Q = 200$ μL/min due to the large channel deformation.

Fig. 3 shows plots of intensities at various flow rates across the microchannel for six different chips. Each datapoint is the value of FL emission intensities spatially averaged over 20 square pixels along the rectangular section in Fig. 2a and the error bars represent one standard deviation. When the flow rate Q is 0 for each chip, no deformation is observed based on the uniform intensities across the channel. Fig. 3a shows the average intensities across the

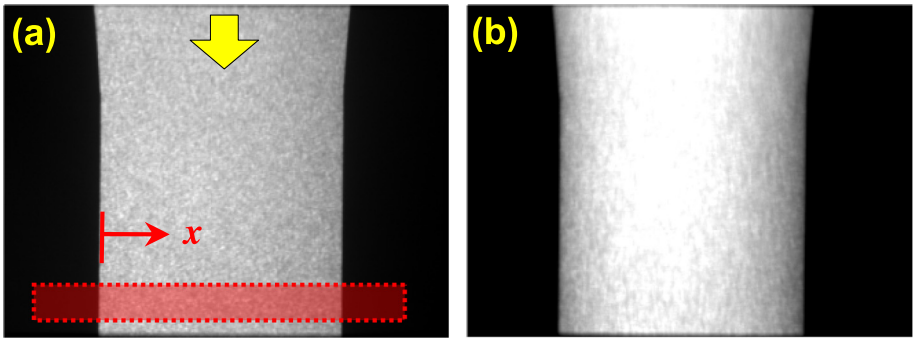

Fig. 2. Fluorescence images of two channels near the inlet reservoir at flow rates $Q = 0$ (a) and $Q = 200$ μL/min (b). The coordinate x that will be used in Fig. 3 starts from left edge of the channel and ends at the other edge, so $x = 0$–500 μm. A yellow arrow shows flow direction. The red doted section indicates the region where fluorescence intensities were measured to investigate channel deformation. Image contrast enhanced for presentation. (For interpretation of the references to color in this figure legend, the reader is referred to the web version of this article.)

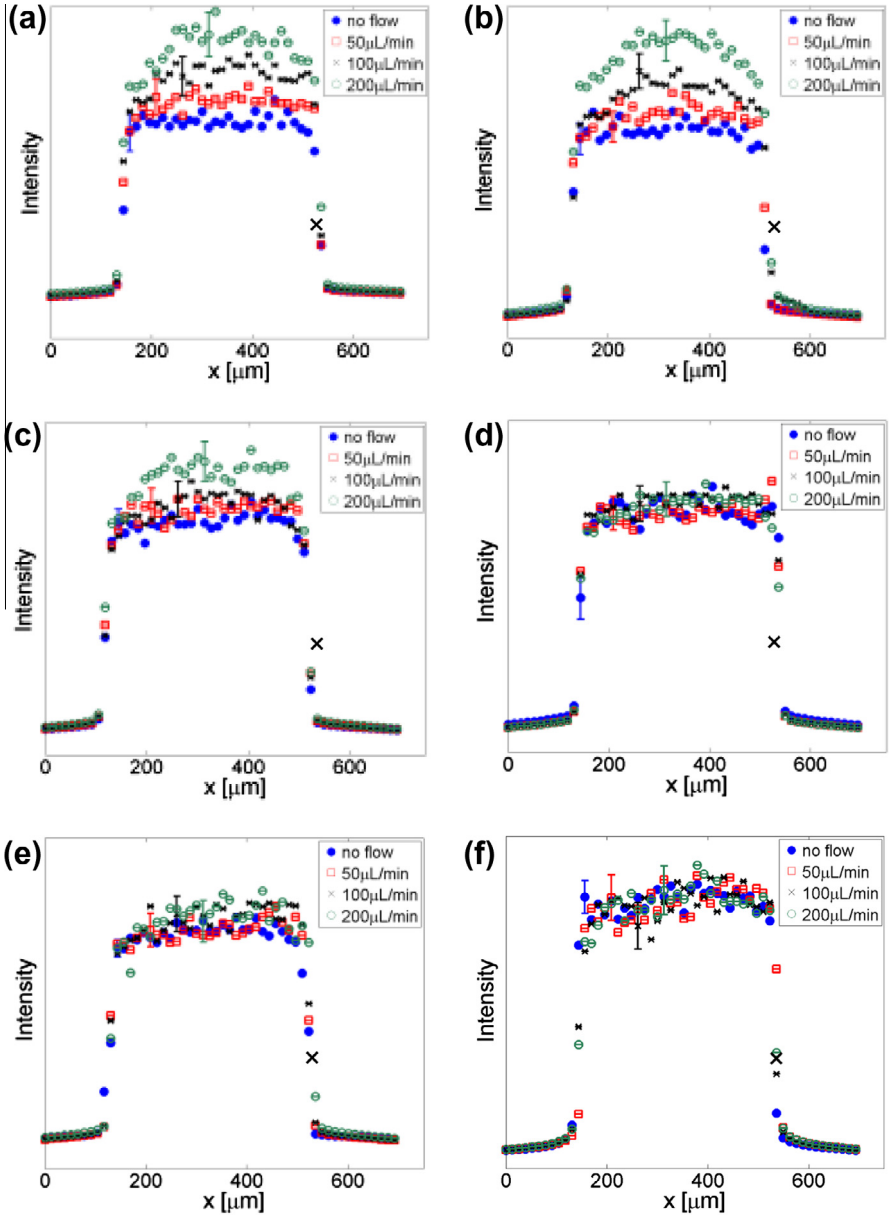

Fig. 3. Plots of fluorescence intensities at flow rates $Q = 0$ (blue solid circles), 50 (red open squares), 100 (black Xs), and 200 (green open circles) across the channel for six different PDMS chips depending on mixing ratios and thermal treatment conditions: M10T0 (a), M5T0 (b), M10T1 (c), M5T1 (d), M10T3 (e), and M5T3 (f). (For interpretation of the references to color in this figure legend, the reader is referred to the web version of this article.)

channel at the flow rates of $Q = 0$, 50, 100, and 200 μL/min, for the M10T0 chip. As the flow rate increases, a higher intensity profile is observed, suggesting that the channel is substantially deformed due to the higher pressure at the higher flow rate. The channel starts to deform at the lowest flow rate of $Q = 50$ μL/min in this test. The maximum of 89.4% change is estimated at the centre of the channel at $Q = 200$ μL/min, which corresponds to the pressure of 167 kPa, when compared at $Q = 0$ μL/min.

Fig. 3b shows the intensity profiles at the same flow rates for the M5T0 chip. As can be seen in the M10T0 chip (Fig. 3a), a similar propensity that the amount of channel deformation increases as the flow rate increases was observed in the M5T0 chip. The absolute percentage of the deformation in the M5T0 chip is 38.2% less at $Q = 50$ μL/min than the M10T0 chip. The deformation at the higher flow rates, however, is same order of magnitude as the M10T0 chip within experimental errors. The deformation at $Q = 50$ μL/min is smaller because the increase in the amount of the curing agent induces the facile displacement of the uncross-linked oligomers and the volatile polymer chains with lower molecular weight to PDMS surfaces, leading to the increase of stiffness and hardness [45–47].

To investigate the thermal effect on the deformation of PDMS channel, we tested two thermally treated 10:1 chips varying the thermal treatment method: (1) M10T1 and (2) M10T3. Fig. 3c and e show the intensity profiles at $Q = 0$, 50, 100, and 200 μL/min for the M10T1 and M10T3, respectively. Compared to the M10T0 in Fig. 3a, the maximum deformation at the centre of the channel was 32 and 53% less at $Q = 100$ and 200 μL/min, respectively, for the M10T1 chip. This improvement was found to be 45 and 46% lower at the same flow rates in the M10T3 chip. These results indicate that thermal treatment is a way to enhance stiffness of PDMS against pressure-induced deformation.

The coupled effect of the thermal treatment and mixing ratio against channel deformation was studied using thermally treated 5:1 chips. Fig. 3d and f show similar experimental results of intensity measurements across the channel in the M5T1 and M5T3, respectively, at various flow rates. Under the same thermal treatment (i.e., Fig. 3a vs. b, c vs. d or e vs. f), the increased use of the curing agent improves the resistance of PDMS to pressure-induced deformation. The higher mixing ratio PDMS shows no deformation of the channel at the highest flow rate of 200 μL/min in this study (Fig. 3f). This is mainly due to the enhanced stiffness of PDMS induced by increases in density and cross-linking [47–49]. Comparing Fig. 3b and d, the thermal treatment of the 5:1 chip also improves the resistance to deformation. For the same flow rate, less channel deformation was observed in the thermally treated channel (Fig. 3d), as compared to the regular 5:1 chip (Fig. 3b). This increase of resistance is most likely due to the fact that thermal aging induces the displacement of the uncross-linked oligomers and the volatile polymer chains to the PDMS surfaces [13,45,46].

Collectively, the increase use of curing agent and thermal treatment play a significant role in the enhancement of PDMS stiffness and its resistance to deformation. The length of the thermal treatment might be another parameter that could further increase the deformation resistance of the PDMS chips. However, it does not appear to have an effect on the deformation of the 5:1 chips. The same order of magnitude deformation is observed for the three-day-treated chip (Fig. 3f) as it is for the one-day-treated chip (Fig. 3d). This is probably due to a saturation of the temperature-based displacement of the uncross-linked oligomers and volatile polymers after one day treatment for the higher curing agent mixture.

Fig. 4 shows average channel deformation at various inlet pressure conditions (i.e., flow rates) for the different types of channels. These values are estimated by normalizing the average discrepancy between the intensities at given flow rate and those under no flow conditions. Note that the intensities under no flow conditions represent the height of the original channel. The largest channel deformation is in the M10T0 chip. Even at the lowest inlet pressure $P = 117$ kPa, 60% deformation was observed. In contrast, the least deformation is in the M5T1 and M5T3. At $P = 165$ kPa, these two channels are deformed only about 7% from its original state. This small deformation was improved up to 860%, as compared to the M10T0 chip. The error bar represents the average percentage based standard deviation of these datapoints.

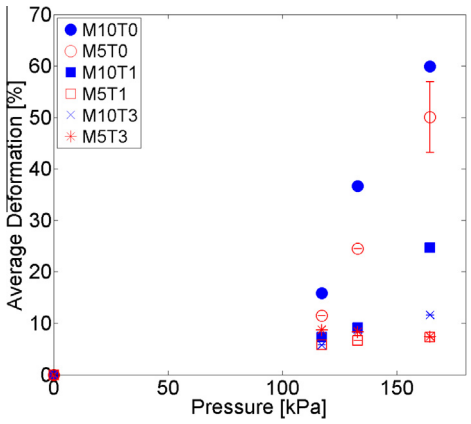

Fig. 4. A plot of average deformation of the PDMS channels at various theoretical inlet pressures for different PDMS chips. Symbols in blue represent data for the 10:1 chips and those in red show data for the 5:1 chips. The error bar shows the average percentage based standard deviation of all datapoints. (For interpretation of the references to color in this figure legend, the reader is referred to the web version of this article.)

3.2. Swelling of PDMS by toluene injection

Another important aspect of PDMS compatibility in microfluidic application is its swelling when in contact with organic solvents because of the growing demand of using PDMS for organic synthesis in organic solvents [32,50]. To study the solvent compatibility of PDMS, the four PDMS chips (M10T0, M5T0, M10T3, M5T1) were prepared. Each chip has microchannel dimensions of either 100 μm in width (W) and 100 μm in height (H) or 500 μm (W) and 30 μm (H). Toluene, which swells PDMS [32], was then allowed to flow through the channel at 20 μL/min using the syringe pump. Then, sequential brightfield images of the channels were taken from $t = 0$ s (initial) to $t = 12$ s (final) to examine the swelling due to the diffusion of toluene into PDMS.

Fig. 5a and d show the brightfield images of the M10T0 and M5T1 microchannels which are initially empty, respectively. These channels are 100 μm in height and 100 μm in width. As toluene was injected continuously, it diffused into the PDMS, leading to variations of the channel shape. Fig. 5b shows the image of the channel in the M10T0 chip at $t = 0.28$ ms after toluene injection. Two thick white lines outside the main fluid channel, indicated by the arrow, show the front end of toluene diffusion into PDMS that induces the swelling, reducing the channel width. At $t = 12$ s the PDMS had further swollen and finally the channel reached its final swollen state (Fig. 5c and see video in ESI†). The channel width was reduced by 55% due to swelling. By contrast, the M5T0 chip shows 30% change in its width, suggesting that increased use of the curing agent has an effect on the improvement of the chemical resistance of PDMS.

The M5T1 chip has the least change in the channel width due to swelling (See video in ESI†). As shown in Fig. 5d–f, only less than 10% change in the profile was observed in the M5T1 chip. Similar results were also obtained for the other 5:1 thermally treated chips. This means that the thermal treatment of cured 5:1 PDMS

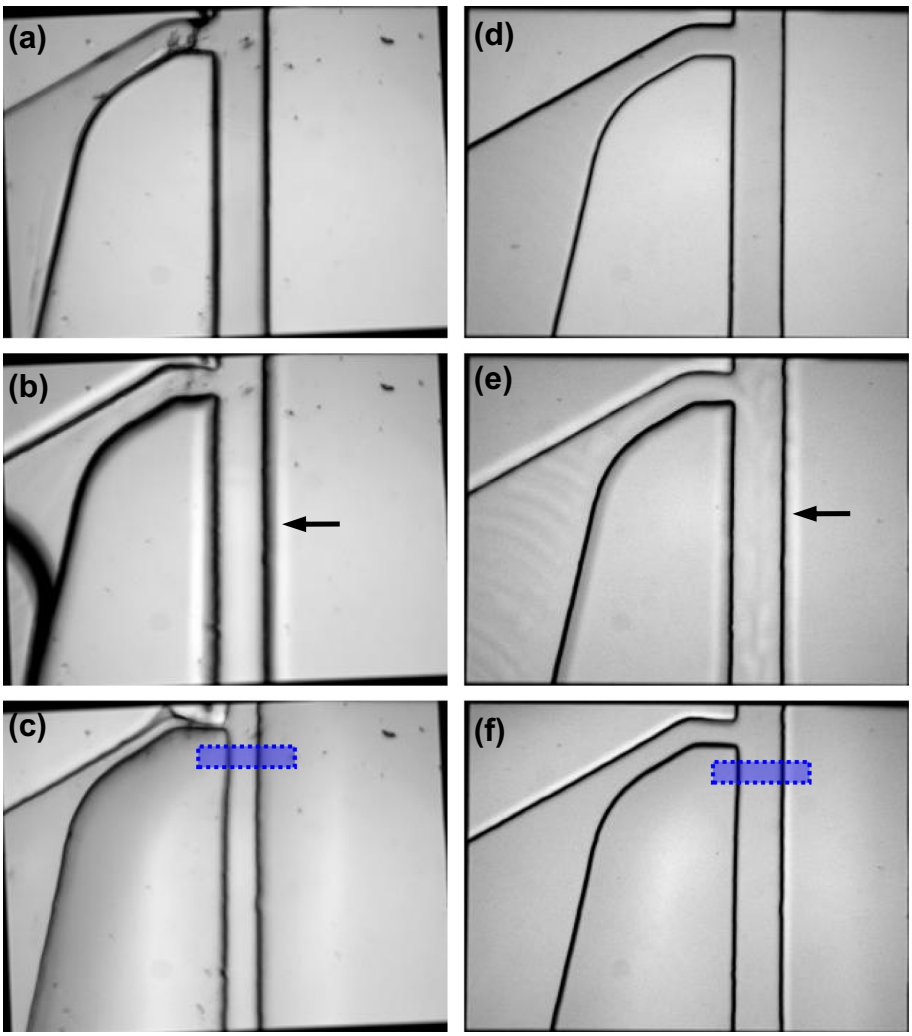

Fig. 5. Sequential optical images of the 100 μm-high PDMS channels with toluene injection at 20 μL/min. (a) An image of M10T0 chip before toluene injection, (b) after t = 0.28 ms, and (c) t = 12 s. Two white lines indicated by an arrow in (b) show the front end of the toluene diffusion to PDMS. Significant deformation due to swelling is observed in (c). (d) An image of the M5T1 chip before toluene injection, (e) after t = 0.28 ms, and (f) t = 12 s. Similar characteristics of toluene diffusion are observed through the movement of the white lines, but there is no significant swelling due to toluene. Blue dotted boxes represent locations where the changes in channel width were estimated. (For interpretation of the references to color in this figure legend, the reader is referred to the web version of this article.)

improves the chemical resistance of PDMS to toluene compared to typical 10:1 PDMS. This increase of resistance is most likely due to the higher mixing ratio and thermal treatment inducing an increase of cross-linking density of PDMS, resulting in reduced surface porosity to organic molecules [13,41,48].

Fig. 6 shows the changes in channel width for the two chips with 500 μm in width and 30 μm in height (See video in ESI†): M10T0 and M5T1. The overall swelling characteristics are similar to the results in Fig. 6a. The maximum reduction of the channel width was 7.5% in the M10T0 chip.

Fig. 7a shows the percentage of the changes in channel width for four PDMS chips with a size of 100 μm in width and 100 μm in height including M10T0 (blue circles), M10T3 (pink crosses), M5T0 (red stars), and M5T1 (black squares). The M10T0 chip has the quickest change of channel profile when toluene was injected. The time constant for the overall changes in the M10T0 chip is 13.9 s when the data are curve-fitted to an exponential function

$$W = W_o e^{-\frac{t}{\tau}} \tag{3}$$

Here, W_o is the original channel width, W is the final width, and τ is the time constant. The larger value of τ, the slower the deformation of the channel. The time constants for the M5T0, M10T3, and M5T1 are 66.7 s, 100.0 s, and 142.9 s, respectively. Collectively, swelling at the higher mixing ratios is slower compared to the standard PDMS chip. In addition, the thermal treatment of 5:1 PDMS further improves chemical resistance to swelling.

Fig. 7b shows the changes in shallower channels with 500 μm in width and 30 μm in height. Similar to Fig. 7a, the M10T0 chip has the quickest change in channel width, showing a 7.5% channel reduction. Due to the plateau region between 2.5 s and 10 s in the M10T0, the time constants for these chips are not estimated for comparison. The final channel widths at t = 12 s were 96.5% and 99% for the M5T0 and M5T1 chips, respectively. These results show qualitatively similar characteristics to those observed for the 100 μm × 100 μm chips in Fig. 7a. The observations from Figs. 5–7 lead to the conclusion that the increased use of curing agent and longer timescales for thermal treatment of the cured PDMS create a synergistic effect for resistance to swelling.

The resistance of the PDMS samples, which includes two chips with a mixing ratio of 10:1 or 5:1, two kinds of thermally treated 10:1 chips, and two kinds of thermally treated 5:1 chips, to toluene was also studied through the measurement of weight change after soaking the samples in toluene. The weight changes by the swelling of the samples are due to weak compatibility of PDMS to toluene [32], and were estimated by measurement of sample weight

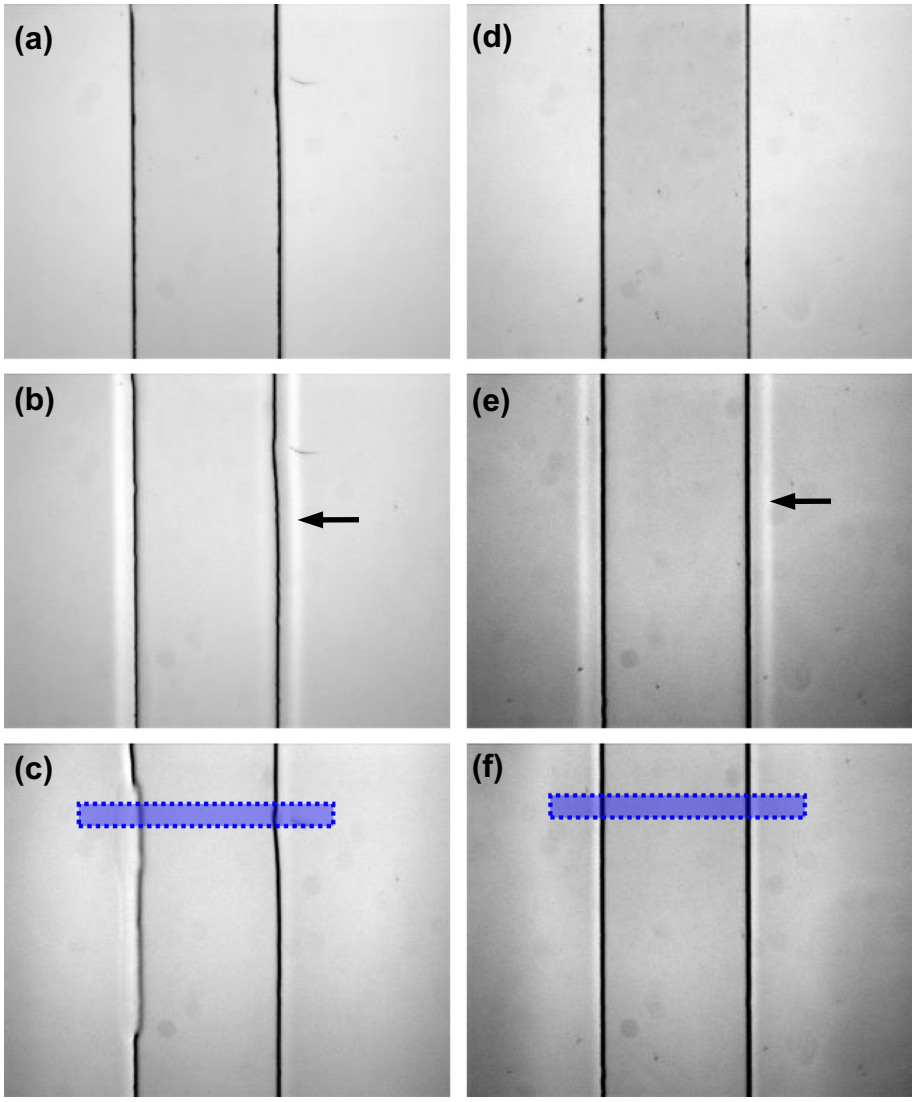

Fig. 6. Sequential optical images of the 30 μm-high PDMS channels with toluene injection at 20 μL/min. (a) An image of the M10T0 before toluene injection, (b) after $t = 0.28$ ms, and (c) $t = 12$ s. (d) An image of the M5T1 chip before toluene injection, (b) after $t = 0.28$ ms, and (c) $t = 12$ s. The overall characteristics of PDMS swelling are similar to results of the 100 μm-high chips in Fig. 5. Blue dotted boxes represent locations where the changes in channel width were estimated. (For interpretation of the references to color in this figure legend, the reader is referred to the web version of this article.)

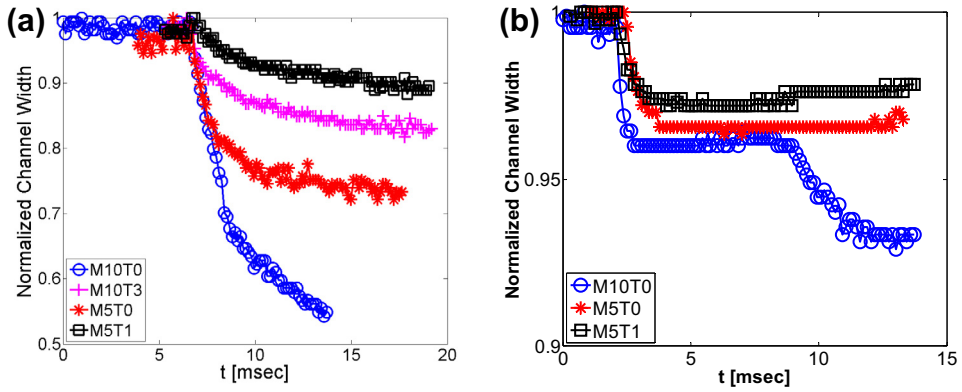

Fig. 7. Changes in channel width of the PDMS chips along with toluene injection for several chips (M10T0, M10T3, M5T0, M5T1) with two different cross-sectional areas: 100 μm in width and 100 μm in height (a) and 500 μm in width and 30 μm in height (b). In both cases, the M10T0 chips are deformed most due to swelling and the M5T1 chip has least deformed, suggesting that this chip has higher chemical resistance. Compared to the shallower channels in (a), the channels with low aspect ratio in (b) swells faster due to the larger exposed surface area (See videos in ESI†).

Table 2
Weight increments of PDMS at different mixing ratios and thermal treatment when it was immersed over 30 min or 1 h. The maximum standard deviation of all data is less than 2%.

Storage time [min]	Mixing ratio (prepolymer: curing agent)					
	M10T0	M10T1	M10T3	M5T0	M5T1	M5T3
30	56.5	28.5	27.5	49.7	26.2	24.1
60	78.6	45.8	43.1	62.1	38.3	32.2

before and after the immersion. Table 2 shows the percentage of weight change of these samples after they were immersed in toluene for 30 min or 1 h. At both soaking timescales, the pure 10:1 PDMS shows the most noticeable weight change, indicating the largest degree of swelling (i.e., the weakest to the solvent). This result agrees with work of Abate et al. [28] study, which showed that 10:1 PDMS significantly swollen when in contact with toluene. The increased use of the curing agent improves the chemical resistance of the 5:1 chips. After 1 h of storage, the M5T0 chip

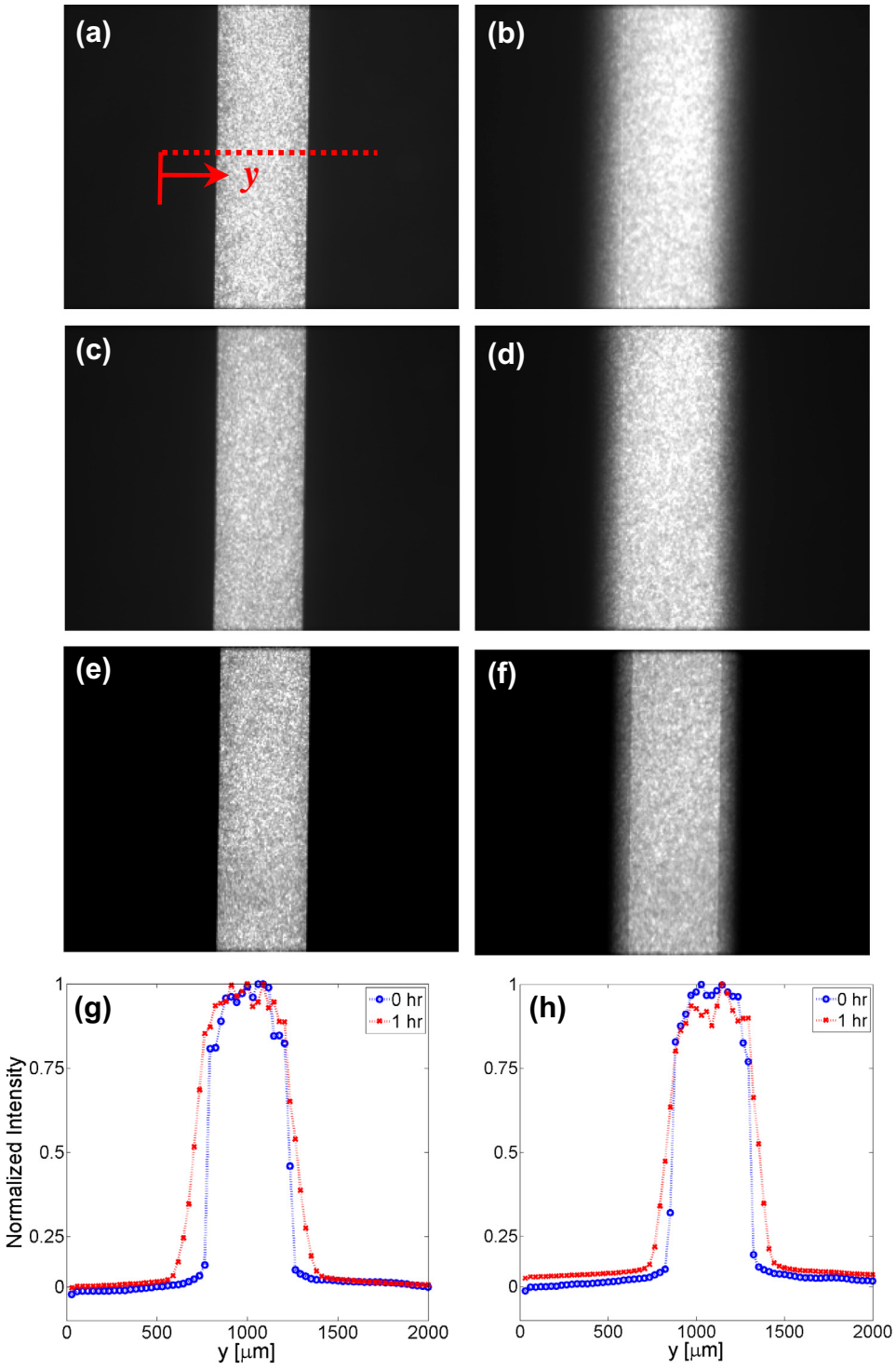

Fig. 8. Fluorescence images of three different PDMS chips at $t = 0$ and 60 min with RhB injection. (a, b) M10T0 chip, (c, d) M5T0 chip, (e, f) M5T1 chip. (g) Normalized intensity profiles at $t = 0$ and 60 min along the line in red (Fig. 8a) for the M10T0 chip. (h) Similar intensity profiles for the M5T1 chip. (For interpretation of the references to color in this figure legend, the reader is referred to the web version of this article.)

was 26% less swollen when compared to the M10T0 chip. The thermal treatment of PDMS further increases its chemical resistance, similar to the observations in the experiments with toluene injection. The M5T1 chip was at least 38% less swollen when compared to the M5T0 chip. However, the longer period of thermal treatment at 200 °C has little effect when the results of the M10T1 and M10T3 or the results of the M5T1 and M5T3 are compared, respectively, in Table 2.

Notably, the remarkable improvement of PDMS on chemical resistance was observed in the M5T3 chip. The combined effect of thermal treatment and increased mixing ratio contributes to the smallest weight gain (i.e., the strongest chemical resistance), 40% and 20% less compared to regular 10:1 PDMS and non-treated 5:1 PDMS, respectively. Thermal treatment temperature also plays an important role in increasing the chemical resistance of PDMS. When treated at 85 °C, the PDMS gains 48.7% weight increase, as compared to 32.2% when treated at 200 °C. Note that the absolute weight increment of the thermally treated PDMS due to swelling is clearly dependent on the timescales of exposure of PDMS to the chemical solvents.

3.3. Diffusion of RhB molecules to PDMS

It is well known that the polymeric microfluidic chips, especially PDMS, have issues of absorption and diffusion of small hydrophobic molecules to their surface and bulk [41,42,51]. Fig. 8 shows fluorescence images of 500 m wide PDMS channels filled with aqueous 100 μM RhB at 0 and 60 min after the solution was injected at 10 μL/min. Three different PDMS chips were employed in the tests: M10T0, M5T0, and M5T1.

Fig. 8a shows fluorescence images of the M10T0 chip at $t = 0$, depicting no initial absorption or diffusion in PDMS. Keeping the solution injected, a large amount of RhB molecules in the solution start to absorb into the surrounding PDMS walls and subsequently penetrate into the PDMS, producing a smoother profile that gradually decreases from the wall to the interior of the sample. After 60 min of RhB injection, significant diffusion of RhB molecules to PDMS was observed as shown in Fig. 8b. These results agree well with previous RhB sorption experiments in 10:1 PDMS chip [28,41,42].

To investigate the possible improvement on absorption and diffusion of RhB to PDMS, we performed the same tests with chips either prepared at the higher mixing ratio or treated thermally. As seen in Fig. 8c and d, there are no significant changes in RhB absorption and diffusion when only increasing use of the curing agent. However, when the 5:1 PDMS was thermally treated at 200 °C, less diffusion of RhB molecules was identified, as shown in Fig. 8f. Some thermally treated chips also show further enhanced blockage of the RhB diffusion to PDMS (See ESI†). Quantitative analysis of the diffusion is possible by comparing two intensity profiles at $t = 0$ and $t = 60$ min (Fig. 8g and h). The amount of diffusion of RhB molecules to PDMS is estimated using the total intensities penetrated into PDMS, which is 30% higher than the background noise. Based on the linear relationship between intensity and concentration, 52% more RhB molecules diffused into the M10T0 chip. Nearly identical results were also observed for the M5T3 chips, suggesting that the long-term thermal aging has no significant effect. Although the thermal treatment and increased use of curing agent can not entirely eliminate the dye diffusion and absorption problem in PDMS, these methods provides a prompt motivation for new research in this direction to alleviate RhB absorption and diffusion.

4. Conclusions

PDMS-based chips have many advantages such as low cost, fast prototyping, and desirable surface properties, making them a leading material in various microfluidic applications. However, deformation-based discrepancies between measured pressure drop or flow rate and theoretical predictions are one of the major challenges in using this material under pressure-driven flow at the microscale. The poor chemical compatibility of PDMS is also of important consideration in a few applications such as organic synthesis. In this paper, we combined and modified two previously isolated fabrication methods to further enhance the material and surface properties of PDMS. It is known that increased use of the curing agent can improve the stiffness and hardness of PDMS up to 40%, which provides better resistance to channel deformation under pressure-driven flow. It is also known that the thermal treatment of cured PDMS can increase its stiffness up to 50%. The higher aging temperature (200 °C) that improves PDMS stiffness faster and more substantially was chosen in this study. We found that the combined processes rendered nonlinear effects on the improvement of material properties and could dramatically enhance PDMS stiffness, showing 860% less deformation in thermally treated 5:1 PDMS channel under pressure-driven flow, as compared to that in the standard 10:1 PDMS channel. With regards to chemical swelling, 10:1 PDMS shows very weak compatibility when in contact with toluene, resulting in 50% change in channel profile. In contrast, the thermally enhanced 5:1 PDMS changed 10% in channel shape, improving its chemical resistance to toluene absorption. The absorption and diffusion of organic molecules into PDMS were also studied by fluorescence imaging of the channel profile over 1 h of RhB injection. The results show that the enhanced PDMS produces 60% improvement on the blockage of dye absorption over the standard M10T0 chip. Collectively these results are quite useful since the thermally treated 5:1 PDMS can serve as an enhanced material in microfluidics that have a stronger resistance to chemicals and deformation.

Acknowledgements

This work was supported by an NSF CAREER Award grant CBET-1151091. We thank Dr. T.J. Kim and Mr. A. Shahriari for their assistance in chip fabrication.

Appendix A. Supplementary data

Supplementary data associated with this article can be found, in the online version, at http://dx.doi.org/10.1016/j.mee.2014.04.041.

References

[1] G.M. Whitesides, E. Ostuni, S. Takayama, X. Jiang, D.E. Ingber, Annu. Rev. Biomed. Eng. 3 (2001) 335–373.
[2] Y. Xia, G.M. Whitesides, Angew. Chem. Int. Ed. 37 (1998) 550–575.
[3] S.R. Quake, A. Scherer, Science 290 (2000) 1536–1540.
[4] T. Fujii, Microelectron. Eng. 61–62 (2002) 907–914.
[5] T.K. Shih, C.F. Chen, J.R. Ho, F.T. Chuang, Microelectron. Eng. 83 (2006) 2499–2503.
[6] J.C. McDonald, D.C. Duffy, J.R. Anderson, D.T. Chiu, H. Wu, O.J.A. Schueller, G.M. Whitesides, Electrophoresis 21 (2000) 27–40.
[7] A.A. Saha, S.K. Mitra, M. Tweedie, S. Roy, J. McLaughlin, Microfluid. Nanofluid. 7 (2009) 451–465.
[8] M. Li, S. Li, J. Wu, W. Wen, W. Li, G. Alici, Microfluid. Nanofluid. 12 (2012) 751–760.
[9] H. Wu, T.W. Odom, D.T. Chiu, G.M. Whitesides, J. Am. Chem. Soc. 125 (2003) 554–559.
[10] G.M. Whitesides, Nature 442 (2006) 368–373.
[11] W.M. Choi, O.O. Park, Microelectron. Eng. 70 (2003) 131–136.
[12] R. Mukhopadhyay, Anal. Chem. 79 (2007) 3248–3253.
[13] M. Kim, B.U. Moon, C.H. Hidrovo, J. Micromech. Microeng. 23 (2013) 095024.
[14] A. Gaspar, M.E. Piyasena, L. Daroczi, F.A. Gomez, Microfluid. Nanofluid. 4 (2008) 525–531.
[15] D. Fuard, T. Tzvetkova-Chevolleau, S. Decossas, P. Tracqui, P. Schiavone, Microelectron. Eng. 85 (2008) 1289–1293.
[16] P. Roca-Cusachs, F. Rico, E. Martinez, J. Toset, R. Farre, D. Navajas, Langmuir 21 (2005) 5542–5548.
[17] Y. Zhang, C.W. Lo, J.A. Taylor, S. Yang, Langmuir 22 (2006) 8595–8601.

[18] T. Lee, O. Mitrofanov, J.W.P. Hsu, Adv. Funct. Mater. 15 (2005) 1683–1688.
[19] T. Gervais, J. El-Ali, A. Gunther, K.F. Jensen, Lab Chip 6 (2006) 500–507.
[20] E. Sollier, C. Murray, P. Maoddi, D. Di Carlo, Lab Chip 11 (2011) 3752–3765.
[21] B.S. Hardy, K. Uechi, J. Zhen, H.P. Kavehpour, Lab Chip 9 (2009) 935–938.
[22] J.G. Curro, J.E. Mark, J. Chem. Phys. 80 (1984) 4521–4525.
[23] Q. Chen, G. Li, Y. Nie, S. Yao, J. Zhao, Microfluid. Nanofluid. (2013), http://dx.doi.org/10.1007/s10404-013-1222-9.
[24] A.H. Shapiro, J. Biomed. Eng. 99 (1977) 126–147.
[25] M. Heil, J. Fluid Mech. 353 (1997) 285–312.
[26] M.A. Holden, S. Kumar, A. Beskok, P.S. Cremer, J. Micromech. Microeng. 13 (2003) 412–418.
[27] G.T. Roman, C.T. Culbertson, Langmuir 22 (2006) 4445–4451.
[28] A.R. Abate, D. Lee, T. Do, C. Holtze, D. Weitz, Lab Chip 8 (2008) 516–518.
[29] B. Kim, L.Y. Hong, Y.M. Chung, D.P. Kim, C.S. Lee, Adv. Funct. Mater. 19 (2009) 3796–3803.
[30] K. Yu, Y. Han, Soft Matter 2 (2006) 705–709.
[31] M. Domenichini, R. Sahai, P. Castrataro, R. Valsecchi, C. Tonelli, F. Greco, P. Dario, Microfluid. Nanofluid. (2013), http://dx.doi.org/10.1007/s10404-013-1187-8.
[32] J.N. Lee, C. Park, G.M. Whitesides, Anal. Chem. 75 (2003) 6544–6554.
[33] R. Dangla, F. Gallaire, C.N. Baroud, Lab Chip 10 (2010) 2972–2978.
[34] Y.J. Park, S.J. Yoo, E.J. Lee, D.H. Lee, J.Y. Kim, S.H. Lee, Biochip J. 4 (2010) 230–236.
[35] J. Zhou, A.V. Ellis, N.H. Voelcker, Electrophoresis 31 (2010) 2–16.
[36] T.C. Riche, B.C. Marin, N. Malmstadt, M. Gupta, Lab Chip 11 (2011) 3049–3052.
[37] G. Sui, J. Wang, C.C. Lee, W. Lu, S.P. Lee, J.V. Leyton, A.M. Wu, H.R. Tseng, Anal. Chem. 78 (2006) 5543–5551.
[38] J.B. Orhan, V.K. Parashar, J. Flueckiger, M.A.M. Gijs, Langmuir 24 (2008) 9154–9161.
[39] H.H. Lin, S.C. Chang, Y.C. Su, Microfluid. Nanofluid. 9 (2010) 1091–1102.
[40] R.L. Smith, C.J. Demers, S.D. Collins, Microfluid. Nanofluid. 9 (2010) 613–622.
[41] M.D. Borysiak, K.S. Bielawski, N. Sniadecki, C.F. Jenkel, B.D. Vogt, J.D. Posner, Lab Chip 13 (2013) 2773–2784.
[42] R. Samy, T. Glawdel, C.L. Ren, Anal. Chem. 80 (2008) 369–375.
[43] B.R. Munson, D.F. Young, T.H. Okiishi, W.W. Huebsch, Fundamentals of Fluid Mechanics, sixth ed., Wiley, 2009.
[44] C.H. Hidrovo, D.P. Hart, Meas. Sci. Technol. 12 (2001) 467–477.
[45] J. Kim, M.K. Chaudhury, M.J. Owen, J. Colloid, Interface 226 (2000) 231–236.
[46] D.T. Eddington, J.P. Puccinelli, D.J. Beebe, Sens. Actuators B 114 (2006) 170–172.
[47] C. Manneschi, P. Fanzio, E. Angeli, G. Firpo, L. Ceseracciu, V. Mussi, L. Repetto, U. Valbusa, Microfluid. Nanofluid. 14 (2013) 21–30.
[48] D. Vesely, Polymer 42 (2001) 4417–4422.
[49] M. Zhu, D. Vesely, Eur. Polym. J. 43 (2007) 4503–4515.
[50] X. Kang, C. Luo, Q. Wei, C. Xiong, Q. Chen, Y. Chen, Q. Ouyang, Microfluid. Nanofluid. 15 (2013) 337–345.
[51] I. Wong, C. Ho, Microfluid. Nanofluid. 7 (2009) 291–306.